

BUILDING SEISMIC STABILITY - CODE PROVISIONS VS. INELASTIC BEHAVIOR

L. Fahnestock¹, S. Shi² & M.S. Speicher³

¹ University of Illinois Urbana-Champaign, Urbana, IL, USA, fnstck@illinois.edu

² University of Illinois Urbana-Champaign, Urbana, IL, USA

³ National Institute of Standards and Technology, Gaithersburg, MD, USA

Abstract: *In a building, seismic stability is provided when the internal restoring forces resist the effective earthquake forces plus the destabilizing effects of gravity that arise when the building displaces laterally. Although this concept can be succinctly stated, its implementation in building code provisions is not as straightforward. For example, many building codes simplify earthquake effects using static design forces that are reduced to consider the influence of inelastic response, and elastic analysis is used to proportion the building structural system. Although this approach has sound justification, it introduces confusion about incorporating the destabilizing effects of gravity, often called second-order or $P-\Delta$ amplification effects. Consideration of $P-\Delta$ effects varies around the world, but in the United States the governing standard on loads stipulates a procedure to amplify structural demands using elastic lateral displacements. Although this simplified strategy, which does not consider inelastic lateral displacements that will occur during a large earthquake, typically leads to a modest increase in strength and stiffness of the building structural system, it is not fundamentally linked to enhanced earthquake performance. The situation is further complicated by other design requirements, such as drift limits and ductile detailing, that may significantly influence strength and stiffness of the building structural system and obscure the $P-\Delta$ amplification aspects of the design process. Recent research on seismic stability behavior and design of steel building systems illustrates the relative influence of key parameters and provides insight into considering $P-\Delta$ effects in a manner that is linked to inelastic earthquake response.*

1. Introduction

A ductile seismic force-resisting system (SFRS) provides significant inelastic deformation capacity through distributed yielding within a favorable global mechanism. Seismic design provisions that employ ductile detailing requirements and capacity-based proportioning are well established and lead to predictable SFRS lateral force-displacement response. It is understood that a SFRS must sustain large inelastic displacements while resisting the destabilizing effects of gravity, and the characteristic behavior of a SFRS under earthquake and gravity loading can be captured using numerical models that include geometric and material nonlinearities. Despite this fact, consideration of seismic stability typically employs elastic models, often in combination with approximate methods. This paper challenges the elastic perspective that underlies typical seismic stability code provisions in the United States and examines potential modifications that would more transparently reflect inelastic stability behavior. In addition, nonlinear inelastic response of steel moment frames and braced frames is used to illustrate the influence of design parameters and SFRS features that are not explicitly designed.

2. Background

2.1. Stability Design

The most common approximate method that is used in seismic design provisions to evaluate and address the destabilizing effects of gravity (P - Δ effects) is the stability coefficient, typically represented by θ . There are various forms of this coefficient, but in general concept, it represents a ratio of the destabilizing effects of gravity acting on the building lateral displacements to the restoring capability of the SFRS. The stability coefficient is derived in the context of a single-story building, and then used to evaluate each story of a multi-story building. The stability coefficient takes the following form, which can be viewed as either a ratio of moments (overturning \div restoring) or stiffnesses (geometric \div restoring):

$$\theta = \frac{P\Delta}{Vh} = \frac{M_{P\Delta}}{M_{Vh}} = \frac{P/h}{V/\Delta} = \frac{k_G}{k} \quad (1)$$

Here, P = gravity load, V = story shear, Δ = story displacement caused by the story shear, h = story height, $M_{P\Delta}$ = overturning moment generated by gravity load, M_{Vh} = restoring moment generated by the story shear, k = story stiffness, and k_G = geometric stiffness. Considering versions of θ that are implemented in seismic code provisions (Ziemian 2010, De Francesco and Sullivan 2023), the primary fundamental distinction is whether elastic or inelastic response is considered.

In the United States, although documents published over two decades ago (FEMA 2000a, 2000b) clearly identified the shortcomings of an elastic stability coefficient – here denoted θ_e – for evaluating seismic stability and proposed an inelastic stability coefficient, an elastic stability coefficient is still used. In ASCE 7, *Minimum Design Loads and Associated Criteria for Buildings and Other Structures* (ASCE 2022), θ_e is checked for every story in a building. If $0.1 < \theta_e \leq \theta_{max}$, P - Δ effects must be determined by “rational analysis,” or forces and displacements in the SFRS are permitted to be multiplied by the elastic amplification factor:

$$AF_e = \frac{1}{1 - \theta_e} \quad (2)$$

In commentary provided by the ASCE 7 background document – the *NEHRP Recommended Seismic Provisions for New Buildings and Other Structures* (NEHRP 2009) – two types of “rational analysis” are identified: nonlinear static pushover analysis and nonlinear dynamic response history analysis. Both of these methods provide direct fundamental assessment of nonlinear seismic stability behavior, but the elastic amplification factor method using θ_e does not. It is fitting that ASCE 7 seems to imply, perhaps unintentionally, that using AF_e is an irrational analysis in comparison to the two methods of rational analysis explicitly named.

Arguably a more rational inelastic stability coefficient approach is available, and implemented in international standards (e.g., National Building Code of Canada and New Zealand Standard 1170.5). In this approach, an inelastic stability coefficient, here denoted θ_{DE} , and associated amplification factor are used to provide increased system strength such that the P - Δ effects at the design earthquake displacement, Δ_{DE} , are neutralized:

$$AF_{DE} = 1 + \theta_{DE} \quad (3)$$

Since the seismic building design process typically employs software platforms that conduct geometrically nonlinear elastic analysis, it is desirable to have an approach for automatically incorporating P - Δ effects at Δ_{DE} , even though the inelastic response that leads to Δ_{DE} is not modeled. A simple solution is to use a stiffness reduction factor SRF_{DE} in the geometrically nonlinear elastic analysis, which approximates the secant stiffness associated with Δ_{DE} . In ASCE 7 parlance, SRF_{DE} can be represented as a ratio of the system overstrength factor, Ω_0 , to the displacement amplification factor, C_d . Thus, in a steel building model, SRF_{DE} would be applied as a modifier on the nominal elastic modulus E . This approach will be illustrated below in a case study.

2.2. Secondary Stiffness

The stability coefficient discussion above relates to initial system stiffness and strength, and ensuring that the P - Δ effects do not compromise the system strength at Δ_{DE} . Although using an approach like AF_{DE} or SRF_{DE} to approximately account for inelastic response is viable and certainly more fundamentally correct than using an

elastic approach like AF_e , it still does not address one of the most important parameters that influences seismic stability – persistent secondary stiffness (MacRae 1994, Gupta and Krawinkler 2000, Fahnestock 2022). Most ductile systems develop distributed yielding response that leads to a reasonable region of positive post-yield stiffness, but this secondary stiffness is not part of the design process, which can be considered a missed opportunity or even a failure of reasoning (i.e., a fallacy). The fallacy does not arise from what the code provisions say, but rather what is omitted. In many instances, secondary stiffness may develop due to system characteristics that are not readily apparent, and it is possible that design decisions that do not violate the code could unintentionally reduce secondary stiffness. This issue will be explored below in a case study.

3. Case Study – Four-Story Building

3.1. Theme Building

The four-story theme office building for this study, depicted in Figure 1, has been adapted from the original floorplan of a 16-story building detailed in the National Institute of Standards and Technology (NIST) Technical Note (TN) 1863-1 and TN 1863-2 (Harris and Speicher 2015a, 2015b). The SFRS frames for this building are designed with steel: two three-bay Special Moment Frames (SMFs) in one direction and two two-bay Special Concentrically Braced Frames (SCBFs) in the orthogonal direction. The building is assumed to be located in Los Angeles, California (33.821° N, 117.818°W), and it is designed based on site-specific spectral response acceleration parameters and the ASCE 7-22 equivalent lateral force (ELF) procedure (ASCE 2022), in conjunction with requisite steel specifications (AISC 2022a, b, c). The analyses for this study were conducted using the OpenSees platform (McKenna *et al.* 2010): elastic analyses for proportioning and nonlinear inelastic analyses (static pushover and dynamic response history) for response assessment.

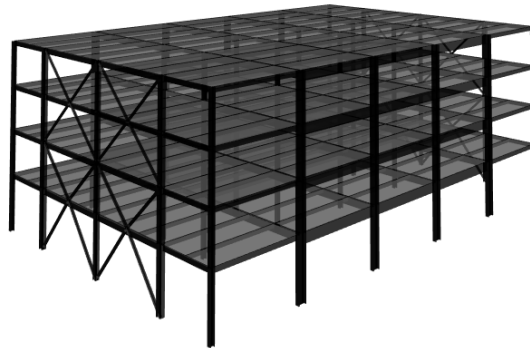


Figure 1. Four-story theme building.

3.2. Nonlinear Numerical Modeling Approach

Considering the placement of the SFRS along the building's perimeter and the intrinsic structural symmetry, a two-dimensional (2D) nonlinear numerical modeling methodology was employed. In all instances, the beams and columns were represented as elastic elements connected to modified Ibarra-Medina-Krawinkler (IMK) hysteretic rotational springs, in accordance with the concentrated plasticity approach. The location of these rotational springs was dependent on the structural system. In the case of an SMF model, the rotational springs were positioned at the ends of the SMF columns (half the column depth away from the face of the beam) and at the center of each reduced beam section (RBS) connection. The force-deformation parameters of the rotational springs adhered to cyclic backbone curves for nonlinear static analyses, while conforming to monotonic backbone curves for nonlinear dynamic analyses, in accordance with the guidelines in a NIST report (NIST 2017). Implementation of this modeling approach also followed recommendation from NIST TN 2084 (Speicher *et al.* 2020). The panel zones in the SMF model were represented at all beam-to-column joints, employing the Krawinkler model (Krawinkler 2000).

In the SCBF model, the rotational springs were placed at the interface between the structural components, namely beams and columns, and the gusset plate rigid links. For braces, displacement-based beam elements with fiber sections were used following the recommendations from Karamanci and Lignos (2014), and the gusset plates were modeled at all beam-to-column-to-brace and beam-to-brace locations (Hsiao *et al.* 2012).

Modal damping (2%) was applied, supplemented by an additional 0.1% stiffness-proportional damping, introduced to mitigate higher modes of vibration. To represent the destabilizing effects of gravity, a leaning column was incorporated into the models. This leaning column was assigned a moment of inertia equivalent to the sum of the moments of inertia of the corresponding tributary columns within the gravity system. Furthermore, to maintain consistency throughout this parametric study, the gravity column orientation (strong-axis vs. weak-axis) was balanced for the building orthogonal directions. Elastic-plastic hinges were defined in the leaning columns at the top and bottom of each story, with flexural strength equivalent to the cumulative plastic moments of the corresponding gravity system columns. This approach approximately captures the interaction between the gravity and lateral systems.

3.3. Influence of Design Variations on SMF Response

Designs Variations

The baseline for this case study is a code-compliant SMF design, denoted as SMF-SO-SD. For this design, the process uses second-order (SO) elastic analysis as required by current stability provisions in ASCE 7-22 and AISC 360-22, and the story drift limit of 2.5% is satisfied (SD). Per AISC 360-22 and the Direct Analysis Method, stiffness is modified using a reduced elastic modulus equal to $0.8E$. Other permutations were considered, including the use of first-order (FO) elastic analysis, ignoring the drift limit (ID) and using an enhanced stiffness reduction within second-order elastic analysis (SO*) in line with the SRF_{DE} concept introduced above. The design matrix of SMFs is summarized in Table 1.

Table 1. Naming convention for SMF design cases.

| Case | Frame Type | Analysis Type | Drift Limit | Stiffness Reduction |
|------------|------------|-------------------|--------------|-------------------------|
| SMF-SO-SD | SMF | Second-Order (SO) | Satisfy (SD) | 0.8 (per AISC DM) |
| SMF-SO-ID | SMF | Second-Order (SO) | Ignore (ID) | 0.8 (per AISC DM) |
| SMF-FO-SD | SMF | First-Order (FO) | Satisfy (SD) | 1 (not relevant for FO) |
| SMF-FO-ID | SMF | First-Order (FO) | Ignore (ID) | 1 (not relevant for FO) |
| SMF-SO*-SD | SMF | Second-Order (SO) | Satisfy (SD) | 3/5.5 (per SRF_{DE}) |

Table 2. Four-story SMF designs.

| Case | Story | Beam | Interior Column | Exterior Column |
|------------|-------|---------|-----------------|-----------------|
| SMF-SO-SD | 4 / 3 | W24X76 | W14X257 | W14X159 |
| | 2 / 1 | W27X94 | W14X311 | W14X193 |
| SMF-SO-ID | 4 / 3 | W24X62 | W14X233 | W14X132 |
| | 2 / 1 | W27X94 | W14X311 | W14X193 |
| SMF-FO-SD | 4 / 3 | W24X76 | W14X257 | W14X159 |
| | 2 / 1 | W27X94 | W14X311 | W14X193 |
| SMF-FO-ID | 4 / 3 | W24X55 | W14X211 | W14X132 |
| | 2 / 1 | W27X94 | W14X311 | W14X193 |
| SMF-SO*-SD | 4 / 3 | W24X76 | W14X257 | W14X159 |
| | 2 / 1 | W27X102 | W14X342 | W14X193 |

Table 2 summarizes member sizes for SMFs and reveals the expected trends, that second-order analysis leads to slightly larger member sizes than first-order analysis (although SMF-SO-SD and SMF-FO-SD are the same since drift controls), and satisfying the drift limit also leads to slightly larger member sizes compared to ignoring the drift limit. The enhanced stiffness reduction in SMF-SO*-SD also increases member sizes slightly compared to SMF-SO-SD.

Static Response

Displacement-controlled nonlinear static analyses were conducted to evaluate and compare the inelastic behavior across the various design cases. Per FEMA P695 (FEMA 2009), the numerical models were subjected to gravity loading equivalent to $1.05D + 0.25L$, with lateral load distribution proportional to the fundamental mode shape. Figure 2 shows the normalized base shear vs. roof drift ratio. On these curves, two points are marked by symbols: a) the end of the linear range, and b) the peak base shear. In addition, the pushover curves change to dotted lines when the maximum story drift anywhere in the frame surpasses 7.5%. This story drift is taken as a nonsimulated collapse, and it aligns with prior research (Speicher *et al.* 2020). In all cases, initial softening occurs around 1% roof drift, followed by more significant softening around 1.5% roof drift. Beyond the peak base shear, a negative stiffness regime manifests due to the global $P-\Delta$ effects.

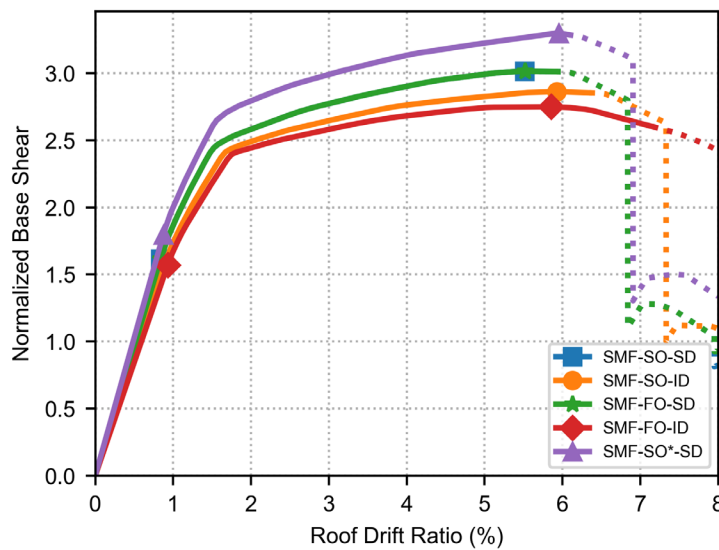


Figure 2. Normalized SMF monotonic static pushover curves.

Table 3 summarizes fundamental period T_1 and three basic response quantities obtained from the pushover analyses: initial stiffness K , overstrength Ω and ductility μ . Overstrength is the ratio of peak base shear to design base shear and ductility is the ratio of ultimate displacement to effective yield displacement. From Figure 2 and Table 3, it is evident that the design variations influence nonlinear response, but not significantly. In general, basic response quantities vary by less than 10% for comparisons between design variations. For designs that satisfy the drift limit (SD), their stiffness and strength are slightly larger than designs that ignore the drift limit (ID). Second-order (SO) analysis used in the design process has little or no influence on the response quantities compared to first-order (FO) analysis used in the design process. When second-order analysis is used in the design process with enhanced stiffness reduction (SO*), member sizes are slightly larger (Table 2) and as a result, the stiffness and strength observed through pushover analysis are also slightly increased (approximately 7% for initial stiffness and 9% for peak strength).

Table 3. Summary of SMF basic response quantities from pushover analyses.

| Case | T_1 (sec) | K (k/in) | Ω | μ |
|------------|-------------|------------|----------|-------|
| SMF-SO-SD | 1.49 | 76.2 | 3.02 | 4.66 |
| SMF-SO-ID | 1.53 | 69.9 | 2.86 | 4.91 |
| SMF-FO-SD | 1.49 | 76.2 | 3.02 | 4.66 |
| SMF-FO-ID | 1.55 | 66.8 | 2.75 | 5.57 |
| SMF-SO*-SD | 1.44 | 81.4 | 3.30 | 4.66 |

Dynamic Response

All design cases were assessed with nonlinear dynamic analyses using the FEMA P695 far-field record set and the associated procedure. This record set comprises twenty-two seismic records (44 individual components) selected from the PEER-NGA database. These ground motions were initially normalized in accordance with FEMA P695 guidelines and then scaled to the risk-targeted Maximum Considered Earthquake (MCE_R) response spectrum at the building's fundamental period. Figure 3 presents the response of the SMFs when subjected to the first record in the dataset, which corresponds to the Northridge earthquake. Considering the similarity in designs, it is not surprising that similar maximum responses are observed across all SMF cases, and this observation for one record is relatively consistent across the far-field record set. Although the maximum responses are similar, residual drifts at the end of the record vary. The SMF-SO-ID case, which ignores the drift limit, has the largest residual drift, whereas the SMF-SO*-SD case has the smallest residual drift. SMF-SO*-SD satisfies the drift limit and was proportioned with enhanced stiffness reduction. Residual drift is not currently a consideration in standard seismic design, but future provisions that are focused on resilience and functional recovery will explicitly evaluate and seek to control residual drift.

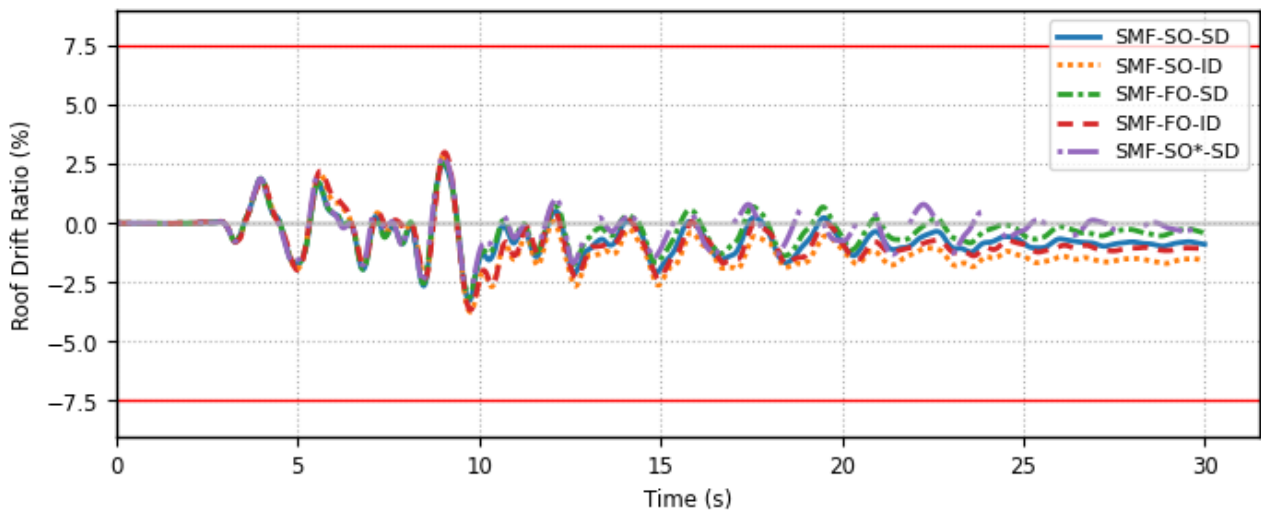


Figure 3. Nonlinear dynamic response for SMFs subjected to MCE_R .

FEMA P695 Collapse Assessment

Incremental dynamic analysis (IDA) was conducted in support of the FEMA P695 collapse assessment, and fragility curves were developed by fitting lognormal cumulative distribution functions (CDFs) to the discrete analysis data points. From the fragility curves in Figure 4, it is evident that the collapse performance is similar for all of the cases considered. However, the collapse performance results presented in Table 4 indicate that the two design cases ignoring the drift limit (SMF-SO-ID and SMF-FO-ID) do not pass the adjusted collapse margin ratio (ACMR) acceptance threshold, whereas the three design cases that satisfy the drift limit do narrowly pass. The collapse performance of the enhanced SMF-SO*-SD case exhibits a small improvement compared to the SMF-SO-SD case, increasing the margin against collapse by approximately 4%.

Table 4. Collapse performance assessment for SMFs.

| Case | CMR | μ | SSF | ACMR | ACMR _{10%} / ACMR | Results |
|------------|------|-------|------|------|----------------------------|---------|
| SMF-SO-SD | 1.48 | 4.66 | 1.34 | 1.98 | 0.99 | Pass |
| SMF-SO-ID | 1.43 | 4.91 | 1.35 | 1.94 | 1.01 | Fail |
| SMF-FO-SD | 1.48 | 4.66 | 1.34 | 1.99 | 0.99 | Pass |
| SMF-FO-ID | 1.32 | 5.57 | 1.38 | 1.82 | 1.08 | Fail |
| SMF-SO*-SD | 1.56 | 4.66 | 1.34 | 2.09 | 0.94 | Pass |

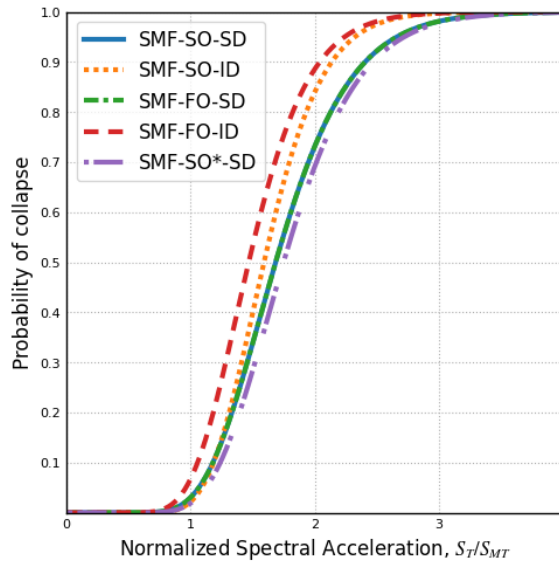


Figure 4. Collapse fragility curves for SMFs.

Overall, these findings align with the observations drawn from nonlinear static response and dynamic MCE-level response. The drift limit appears to have a larger impact than the consideration of $P-\Delta$ effects for these low-rise SMFs. This observation is consistent with the findings of a previous study (Fahnestock *et al.* 2020). All results collectively suggest that the current code provisions, encompassing second-order analysis and drift limit considerations, do not substantially impact design outcomes and seismic performance for the frames studied. Although the SMF-SO*-SD case does not have an appreciably different design or performance than the current code-based design (for the theme building considered), it does contain a more rigorous and transparent treatment of the $P-\Delta$ effects, by targeting amplification associated with the gravity loads acting on the lateral deflections at the design earthquake.

3.4. Influence of Secondary Stiffness on SCBF Response

Seismic Designs

For the present case study of SCBFs, application of the design variations described previously for SMFs – specifically comparing first-order analysis with second-order analysis and considering or ignoring the drift limit – yielded consistent member selections (no changes at all). This consistency suggests that the influence of elastic second-order effects on these stiff 4-story SCBFs can be considered negligible. Furthermore, the observation that ignoring the drift limit results in identical designs shows that the strength-controlled designs inherently satisfy the drift limit criteria. The member section sizes are shown in Table 5.

Table 5. Special concentrically braced frame design.

| Story | Beam | Interior Column | Exterior Column | Brace |
|-------|---------|-----------------|-----------------|------------|
| 4 | W24X76 | W14X68 | W14X68 | HSS5X5X3/8 |
| 3 | W24X76 | W14X68 | W14X68 | HSS6X6X1/2 |
| 2 | W27X102 | W14X132 | W14X145 | HSS7X7X1/2 |
| 1 | W27X102 | W14X132 | W14X145 | HSS7X7X5/8 |

The SCBF system comprises both a primary and secondary structural system, each contributing to the overall lateral load resistance mechanism. The primary system of SCBF is a vertical concentric truss system. This truss system efficiently carries seismic loads through the axial capacities of the braces. The secondary system is not designed and it primarily comes into play after brace buckling and fracture have occurred. It is moment frame action, characterized by flexure of braced frame beams and columns. This secondary system naturally provides secondary stiffness to the structure, along with contribution from the gravity framing.

To evaluate the impact of the inherent secondary stiffness within the SCBF system, three distinct structural configurations were considered. They are all the same basic SCBF design, but with modest changes in the way they are modeled. The first two configurations represent the bounds of realistic SCBF conditions, and the third is a hypothetical case to illustrate the importance of frame action in SCBF seismic performance. The first configuration, denoted as SCBF-Max, is characterized by the maximum framing action from all beams and columns, where all beam-column joints are rigid and the column splices can develop the plastic moment of the column. The second configuration, referred to as SCBF-Min, remains code-compliant but significantly alters the framing action. The beams-column joints transfer close to zero moment and framing action is limited to the columns. Additionally, the column splices, located at approximately one-third of the story height above the floor below, can develop half of the plastic moment of the column. The third configuration, named SCBF-Truss, is not realistic since all joints in the braced frame are defined to be pins, providing essentially no framing action. This results in structural behavior reminiscent of a truss system.

Static Response

Figure 5 shows the normalized pushover curves for the three SCBF cases described above. These curves incorporate a dotted line segment, marking where story drift exceeds the nonsimulated collapse limit, set at 5% for SCBFs. For all cases, there is elastic response up to around 0.2% roof drift, where there is notable softening. From that point, the inelastic behavior displays distinctive characteristics among the three considered SCBF configurations. SCBF-Max exhibits the largest normalized base shear, whereas SCBF-Min records the highest roof drift corresponding to the largest normalized base shear. In contrast, SCBF-Truss reaches its maximum base shear at a much smaller roof drift, not much beyond the end of the elastic range, before experiencing a global negative stiffness.

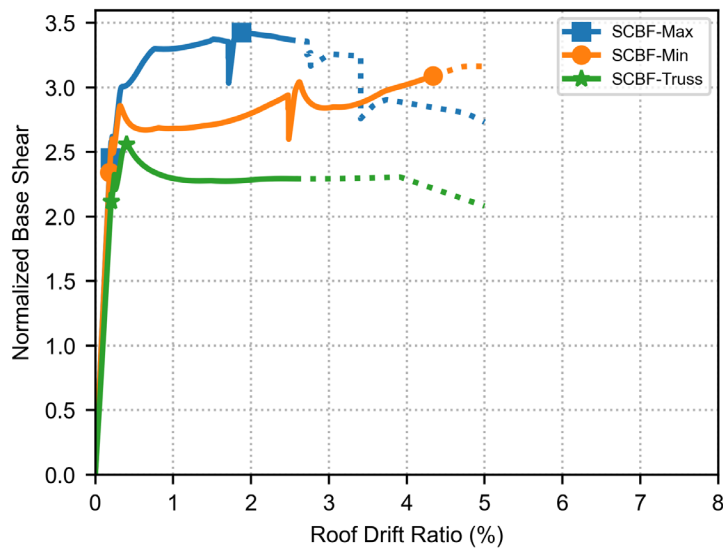


Figure 5. Normalized SCBF monotonic static pushover curves.

Table 6 provides a summary of key response quantities extracted from the pushover analyses conducted on one SCBF. SCBF-Max demonstrates a large overstrength of 3.43 and the largest stiffness, while SCBF-Min exhibits a lower overstrength of 3.09. In contrast, SCBF-Truss has the lowest initial elastic stiffness of the three cases and it exhibits negative global stiffness early in the response.

Table 6. Summary of response quantities of one perimeter SCBF from pushover analyses.

| Case | T_1 (sec) | K (k/in) | Ω | μ |
|------------|-------------|------------|----------|-------|
| SCBF-Max | 0.49 | 961 | 3.43 | 5.55 |
| SCBF-Min | 0.49 | 750 | 3.09 | 10.7 |
| SCBF-Truss | 0.49 | 711 | 2.56 | 4.97 |

Dynamic Response

The three SCBF configurations were subjected to the 44 ground motions from the FEMA P695 far-field record set and the median peak roof drift ratios were computed for each case. For SCBF-Max, the median peak roof drift ratio was 1.35, while SCBF-Min recorded a slightly lower value of 1.19. In contrast, the SCBF-Truss configuration had a median peak roof drift ratio of 1.41. Figure 6 shows the nonlinear dynamic response of the SCBFs when subjected to the first record in the FEMA P-695 set (a Northridge earthquake record). The SCBF-Max and SCBF-Min configurations reach maximum roof drifts of approximately 2%, but do not collapse. In contrast, the SCBF-Truss configuration drifts beyond 5% and becomes unstable.

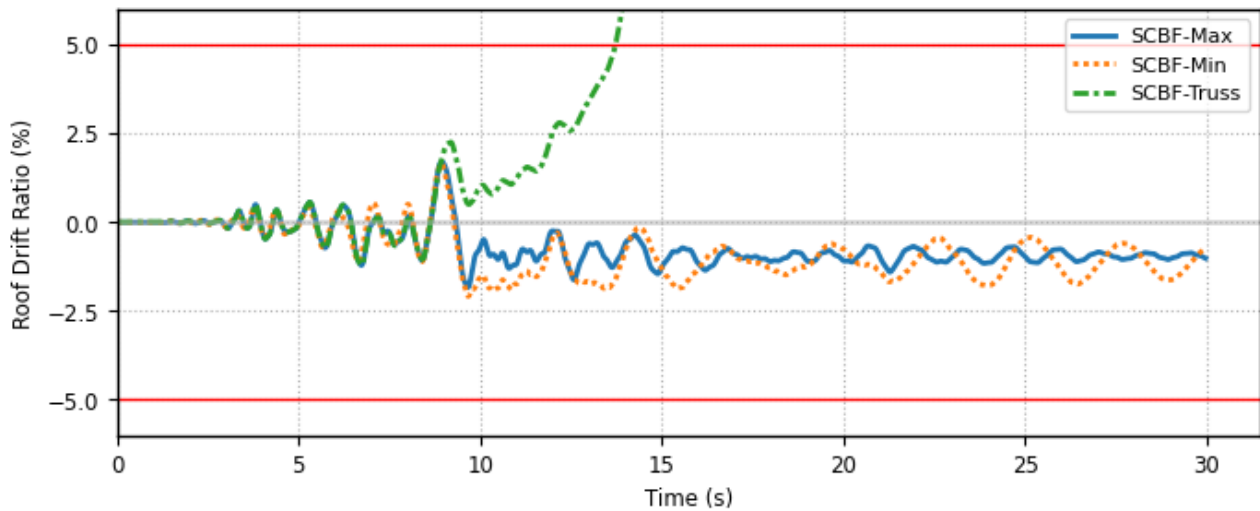


Figure 6. Nonlinear dynamic response for SCBFs subjected to Northridge earthquake record.

FEMA P695 Collapse Assessment

A FEMA P695 collapse assessment was also conducted for the three SCBF configurations. Discrete analysis data and the associated fitted fragility curves are shown in Figure 7. For SCBF-Max and SCBF-Min, the fitted lognormal CDFs provide a reasonable fit for the discrete data points, as demonstrated in many prior studies of ductile SFRS. However, for SCBF-Truss, the lognormal CDF does not fit the data well, owing primarily to collapses at low scale factors for approximately a quarter of the earthquake records. These collapses that occur significantly below the MCE level occur as a result of the more brittle SFRS behavior found in SCBF-Truss. Although brace buckling and yielding initially provide ductility, after the braces in a story experience cyclic degradation, there is little to no story shear resistance remaining. As a result, the system collapse behavior is very sensitive to the properties of earthquake records and the influence that they have on cyclic brace degradation. This specific case study also illustrates the more general point that a SFRS with the potential for primary system degradation and without a robust secondary system will exhibit significant seismic response uncertainty.

Notwithstanding the poor fragility curve fit for SCBF-Truss, the fragility curve comparisons provide insight into the relative behavior of the three SCBF configurations. Qualitatively, as the moment frame action increases (moving from SCBF-Min to SCBF-Max), the fragility curve shifts to the right, indicating more resistance to collapse. In contrast, if no moment frame action is considered (SCBF-Truss), the resistance to collapse is diminished. The irony (or fallacy) is that design provisions do not directly capture this essential behavior; two equally viable designs can have drastically different performance. Though this outcome is not surprising, juxtaposed next to the relatively minor influence the current stability provisions have on the seismic design and associated performance, it can be argued that the design process may in some respects proverbially “miss the forest for the trees.”

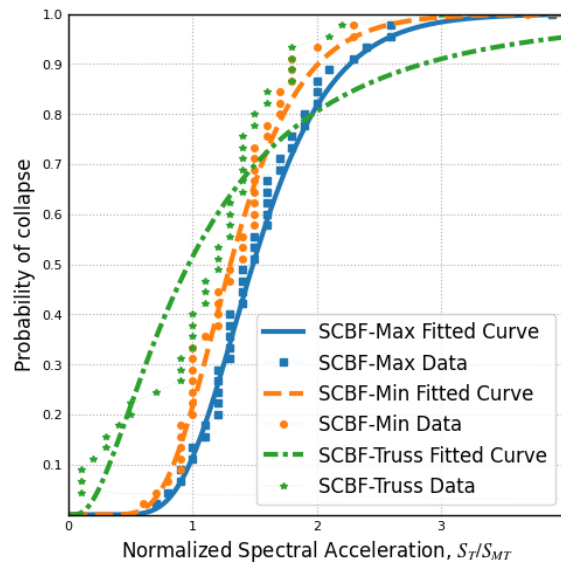


Figure 7. Collapse fragility curves for SCBFs.

Table 7 summarizes collapse assessment for the three SCBF configurations and shows that none of the configurations pass the FEMA P695 performance criterion of 10% probably of collapse given the MCE_R ($ACMR_{10\%}$), although SCBF-Max is only slightly over the acceptance threshold. The most important point for this case study is the significant change in performance when the secondary frame action is removed (SCBF-Truss). In this case, the $ACMR_{10\%}/ACMR$ ratio increases by approximately 40% compared to the SCBF-Max case, indicating the major influence that secondary frame action has on braced frame seismic performance.

Table 7. Summary of collapse performance assessment for the SCBFs.

| Case | CMR | μ | SSF | ACMR | $ACMR_{10\%} / ACMR$ | Results |
|------------|------|-------|------|------|----------------------|---------|
| SCBF-Max | 1.40 | 5.55 | 1.29 | 1.80 | 1.09 | Fail |
| SCBF-Min | 1.27 | 10.7 | 1.36 | 1.73 | 1.13 | Fail |
| SCBF-Truss | 1.25 | 4.97 | 1.27 | 1.59 | 1.54 | Fail |

4. Summary

This paper critically evaluated the elastic perspective that underlies typical seismic stability code provisions in the United States and examined potential modifications that would more transparently reflect inelastic stability behavior. The essential point is that consideration of $P-\Delta$ effects at elastic drift levels is not rational, but instead they must be considered at inelastic drift levels associated with the design earthquake (or perhaps even the maximum considered earthquake). This consideration can be accomplished in the design process through elastic analysis with an inelastic stability coefficient or a comparable stiffness reduction factor. A case study of steel special moment frames demonstrated that for many ductile seismic force-resisting systems (SFRS), consideration of $P-\Delta$ effects at inelastic drifts compared to elastic drifts does not have a significant influence on system proportioning. However, using inelastic drifts in the design process provides more rigor and transparency, and for some types of SFRS and taller buildings, there may be more significant $P-\Delta$ amplification and impact on SFRS proportioning.

A case study for steel special concentrically-braced frames illustrated that post-yield behavior and secondary stiffness are critical parameters that influence seismic stability, yet they are typically not considered directly in seismic design. Many SFRS have intrinsic secondary stiffness that provides seismic stability without intervention by the design engineer, but there may also be ductile SFRS that could be code compliant, yet also possess low secondary stiffness due to design choices that inadvertently reduce secondary stiffness. Evaluation of secondary stiffness as a standard part of the design process is a potential future enhancement, which can be accomplished with relative ease using nonlinear static pushover analysis.

5. Acknowledgments

This study is partially supported by the American Institute of Steel Construction and the National Science Foundation (CMMI 2135686). The opinions, findings, and conclusions in this paper are those of the authors and do not necessarily reflect the views of those acknowledged here.

6. References

- AISC (2022a), *Prequalified Connections for Special and Intermediate Steel Moment Frames for Seismic Applications (ANSI/AISC 358-22)*, American Institute of Steel Construction. Chicago, IL.
- AISC (2022b), *Seismic Provisions for Structural Steel Buildings (ANSI/AISC 341-22)*, American Institute of Steel Construction. Chicago, IL.
- AISC (2022c), *Specification for Structural Steel Buildings (ANSI/AISC 360-22)*, American Institute of Steel Construction. Chicago, IL.
- ASCE (2021), *Minimum Design Loads and Associated Criteria for Buildings and Other Structures, ASCE/SEI 7-22*, American Society of Civil Engineers, Chicago, IL.
- Fahnestock, L. (2022), 'Seismic stability from low ductility to enhanced resilience', *ce/papers* **5**(4), 22–27. <https://doi.org/10.1002/cepa.1723>
- Fahnestock, L., Shi, S. & Speicher, M. S. (2020), Seismic stability assessment of steel moment frames and implications for design, in 'Proceedings of the 17th World Conference on Earthquake Engineering', Vol. 2b-0153, Sendai, JP, pp. 1–12. <https://wcee.nicee.org/wcee/article/17WCEE/2b-0153.pdf>
- FEMA (2000a), *Recommended Seismic Design Criteria for New Steel Moment-Frame Buildings, FEMA-350*, Federal Emergency Management Agency.
- FEMA (2000b), *Systems Performance of Steel Moment Frames Subject to Earthquake Ground Shaking, FEMA-355C*, Federal Emergency Management Agency.
- FEMA (2009), *Quantification of Building Seismic Performance Factors. FEMA P695*, Federal Emergency Management Agency, Washington, D.C.
- Francesco, G. D. & Sullivan, T. J. (2023), 'Improved estimation of p-delta effects on the response of bilinear sdof systems', *Earthquake Spectra* **39**(2), 889–913. <https://doi.org/10.1177/87552930221146569>
- Gupta, A. and Krawinkler, H. (2000) "Dynamic P-Delta Effects for Flexible Inelastic Steel Structures," *J. Struct. Eng.*, ASCE 126 (1): 145-154.
- Gupta, A. & Krawinkler, H. (2000), 'Dynamic p-delta effects for flexible inelastic steel structures', *Journal of Structural Engineering* **126**(1), 145 – 154. [https://doi.org/10.1061/\(ASCE\)0733-9445\(2000\)126:1\(145\)](https://doi.org/10.1061/(ASCE)0733-9445(2000)126:1(145))
- Harris, J. & Speicher, M. S. (2015a), Assessment of first generation performance- based seismic design methods for new steel buildings, volume 1: Special moment frames, Technical Note 1863-1, National Institute of Standards and Technology, Gaithersburg, MD. <https://doi.org/10.6028/NIST.TN.1863-1>
- Harris, J. & Speicher, M. S. (2015b), Assessment of first generation performance- based seismic design methods for new steel buildings, volume 2: Special concentrically braced frames, Technical Note 1863-2, National Institute of Standards and Technology, Gaithersburg, MD. <https://doi.org/10.6028/NIST.TN.1863-2>
- Hsiao, P. C., Lehman, D. E. & Roeder, C. W. (2012), 'Improved analytical model for special concentrically braced frames', *Journal of Constructional Steel Research* **73**, 80–94. <https://doi.org/10.1016/j.jcsr.2012.01.010>
- Karamanci, E. & Lignos, D. G. (2014), 'Computational approach for collapse assessment of concentrically braced frames in seismic regions', *Journal of Structural Engineering* **140**(8), A4014019. [https://doi.org/10.1061/\(ASCE\)ST.1943-541X.0001011](https://doi.org/10.1061/(ASCE)ST.1943-541X.0001011)
- Krawinkler, H. (1978), 'Shear in beam-column joints in seismic design of steel frames', *Engineering Journal* **15**(3), 82–91.
- MacRae, G. A. (1994), 'P- Δ effects on single-degree-of-freedom structures in earthquakes', *Earthquake Spectra* **10**(3), 539–568. <https://doi.org/10.1193/1.1585788>

- McKenna, F., Scott, M. H. & Fenves, G. L. (2010), 'Nonlinear finite-element analysis software architecture using object composition', *Journal of Computing in Civil Engineering* **24**(1), 95–107. [https://doi.org/10.1061/\(ASCE\)CP.1943-5487.0000002](https://doi.org/10.1061/(ASCE)CP.1943-5487.0000002)
- NIST (2017), *Guidelines for nonlinear structural analysis and design of buildings. part IIa - steel moment frames*, NIST GCR 17-917-46v2, National Institute of Standards and Technology, Gaithersburg, MD. <https://doi.org/10.6028/NIST.GCR.17-917-46v2>
- Speicher, M. S., Dukes, J. D. & Wong, K. K. F. (2020), Collapse risk of steel special moment frames per fema p695, Technical Note 2084, National Institute of Standards and Technology, Gaithersburg, MD. <https://doi.org/10.6028/NIST.TN.2084>
- Ziemian, R. (2010), *Guide to Stability Design Criteria for Metal Structures*, 6th Edition, John Wiley & Sons.